International Journal on Engineering Technologies and Informatics

Mechanical Aspects of Hot Tear Formation of Al-Cu Binary Alloys

Research Article

Volume 5 Issue 3- 2024

Author Details

*Xiaoxian Xu[1], Bing Yang[2], Jianchun Wu[2], Yu Zeng[2], Jinyan Liu[2], Damian McGuckin[3], Allen Chhor[3], David St-John[1], Matthew Dargusch[1] and Gui Wang[1]**

[1]*School of Mechanical and Mining Engineering, The University of Queensland, Australia*

[2]*Central Research Institute, Baowu Steel Group Corp Ltd, China*

[3]*Pacific Engineering Systems International, 20D Grose St, Australia*

*Corresponding author

Gui Wang, School of Mechanical and Mining Engineering, The University of Queensland, St Lucia, QLD 4072 Australia

Article History

Received: July 13, 2024 Accepted: July 17, 2024 Published: July 17, 2024

Abstract

Driven by ever increasing structural light-weighting demands of the transport sector and a desire/need to even better understand the complex behaviour of certain casting processes with Aluminium alloys, the hot tearing susceptibility of Al-Cu binary alloys with a solute content of 0.5, 3.0, and 5.0wt% Cu has been investigated through physical experiments and numerical simulations, i.e. virtual experiments. Both the temperature at the hot spot, the designed critical point for hot tearing, and the load at the end of the test bar, have been measured in the physical experiments and compared with the simulation results. The test samples with 0.5 and 3.0 wt% Cu showed hot tears while those with 5.0wt% Cu had no sign of such tearing. The simulations performed with the ProCAST virtual casting software tool have duplicated well the temperature and the trend in the load development seen in the physical experiments. The evolution of the solid fraction, strain rate, strain, stress, and hot tearing indicator has been investigated in detail to reveal the correlation between the physical and numerical experiments.

Keywords: Hot Tearing; Al Cu Binary Alloys; Plastic Strain; Numerical Simulation; Metal Casting

Introduction

In the transport sector, energy conservation and emissions reduction are today's top priorities as the sector addresses sustainable development. Structural light-weighting is one of the most efficient techniques for achieving these goals [1,2]. With one (material) solution to reducing weight in a structure being the use of aluminium and its alloys [3-6], this demand for light-weighting in this sector is set to significantly grow the demand for aluminium alloys (or Al-alloys). Indeed, it has been reported that the overall weight of a rail carriage-body has been halved due to the extensive use of wrought Al-alloys in replacing steel in this structure [7]. Casting is the most common manufacturing process used to create Al-alloy parts in this sector. Aluminium and its alloys have a much higher thermal expansion coefficient than other metals used for structural parts like steel. Because of this, the stress related defects due to thermal contraction during (the solidification and cooling within) a casting process is normally higher than the same defects in those other metals [8]. As the size of a shape casting or a DC casting ingot increases, so too does its thermal stress. This may lead to distortion, cold cracking, or hot tearing. It is this hot tearing, the undesired formation of irregular cracks that develop during the solidification of these castings [8,9], that is the focus of this paper.

It is well accepted that the cause of such hot tearing is generally attributed to the development of thermally induced tensile stresses and strains in a casting as the metal contracts during the late stage of solidification and solid-state shrinkage. Factors contributing to the formation of hot tearing include mushy zone deformation, liquid metal feeding and the supersaturation of vacancies [10-13]. The solidified grains are surrounded by liquid films during the late stage of solidification, and consequently, these semi-solid materials exhibit quite low strength and ductility [14]. How all these interact will depend on the mechanical properties of the alloy in the mushy zone because they determine the ability of the solidifying metal to retain its shape and transfer forces.

Al-Cu alloys have been investigated by numerous researchers [15-25] revealing that hot tearing susceptibility follows a lambda curve relationship when hot tearing severity is correlated to the solute content. They show that Al-0.5wt%Cu and Al-1wt%Cu alloys have the highest hot tearing susceptibility, and that susceptibility decreases as the Cu content increases [16-19]. Studies also demonstrated the influence of Cu concentration, superheating and the amount of eutectic on hot tearing susceptibility [17-21]. All these variables play a significant role in the formation and development of hot tearing. Indeed, Li et al. [26] note that grain size has a large impact on their formation. Viano [19] reported that at a low solute level (0.5wt% Cu), the grain size of the aluminium alloy without grain refinement is more than 5mm and there are very few grain boundaries perpendicular to the direction of strain. The higher hot tearing susceptibility at lower Cu contents can be ex-

plained by the presence of coarser grains, the extent of the mushy zone, a larger linear contraction and there being less residual liquid available for feeding (for example) the non-equilibrium eutectics [12]. The granular model demonstrates that the grain size has a large effect on the 'overpressure' required to overcome the capillary forces at the liquid–void interface. Because of this dependence, the hot tearing susceptibility increases with grain size [27]. However, even grain refined Al-Cu shows severe hot tearing, indicating that hot tearing is a complex and alloy-dependent phenomenon with many variables influencing its formation [19].

This research seeks an enhanced understanding of the mechanical aspects of the Al-Cu alloys on the hot tearing formation, largely by investigating the correlation between the development of stress and strain, and the formation of hot tearing. Most of the experiments were performed virtually, i.e. by numerical simulation with a finite element analysis (FEA), appropriately validated by judiciously chosen physical experiments. Those previously mentioned mechanical properties parameterise the constitutive equations at the heart of the numerical model that will be used to investigate hot tearing during solidification. Therefore, knowledge (to some precision) of these properties is crucial to the performance of the virtual experiments done with that numerical model [15-17].

A virtual prototyping approach was used for the experiments. The validation of each of the cases investigated numerically was done with a single physical experiment, the underlying principal behind virtual prototyping or simulation based engineering to give it another name. This greatly saves on the cost in time, manpower and material of what would otherwise been an expensive set of physical experiments, with the variations all being done numerically. The closeness seen in the results of these two approaches in casting environments over the past 30 years has long given us the confidence that this approach is sound. Indeed, if we find that our physical experiment does not agree with our numerical experiments, it is more likely that the simulation of the casting process may have overlooked an experimental parameter and/or boundary/loading conditions in the numerical model.

Experimental and FEA Model

Experimental Procedure

A modification of the hot tearing test rig reported elsewhere [16,19,20] was used in this study. Figure 1 shows a picture of the casting and a schematic plan view of the mould. The steel mould (a medium carbon steel AISI1026) has a combined centre pouring reservoir and riser that feeds the centres of two test bars. This creates a hot spot and feeder into the centre of bars. Anchoring the two ends of a cast bar produces tensile stresses within it. One bar is restrained from both ends and is used to observe hot tears. The other bar has one end restrained and its other end connected to a load cell and is used for data collection (load and temperature). A type K thermocouple located in the hot spot is used to measure that temperature. As indicated in Figure 1a, the mould was lined with ceramic fibre insulation in specified areas to assist in producing the designed directional solidification. A ceramic fibre paper (of 2mm thickness) was used on the top surface of the mould. A boron nitride coating (Pyrotek PM 6040) covered the rest of the mould surface. A Foseco insulation sleeve with a density of 0.5 kg/m3 (Kalmin-60) was used for the riser. This provided a metalostatic head to supply feed material to the cast bars during solidification and to assist in mould filling. The riser also served as a sprue.

Hot tearing experiments were performed on three Al-Cu binary alloys: 0.5 wt%Cu, 3.0 wt%Cu, and 5.0 wt%Cu. The alloys were prepared from a commercially pure aluminium (99.96%) and pure copper (99.999%) using an induction furnace in a 5kg batch, melted in 780^{0}C, held for 15 minutes, and then poured into the ingot mould. The alloy was remelted using an induction furnace at 750^{0}C, held for 10 minutes, and once it reached 720^{0}C, poured into the preheat mould (200^{0}C). A K-type thermocouple (0.25mm diameter wire with 310 stainless steel sheath) conformed to ANSI specification has been installed in the center of the test bar (the hot spot), the standard of error is 1.1°C (0r 0.4%) in the range of -40°C to 1100°C. A load cell (HYLY-019) was attached to the slide block at the end of the test bar as shown in Figure 1b. It has a measuring range of 0-1000 N, ±0.5%F.S. in accuracy, and 1.0-1.5mv/v in resolution. A data acquisition unit with 8 channels was used to record temperature and load. After casting, the cast bars were visually examined for hot tears.

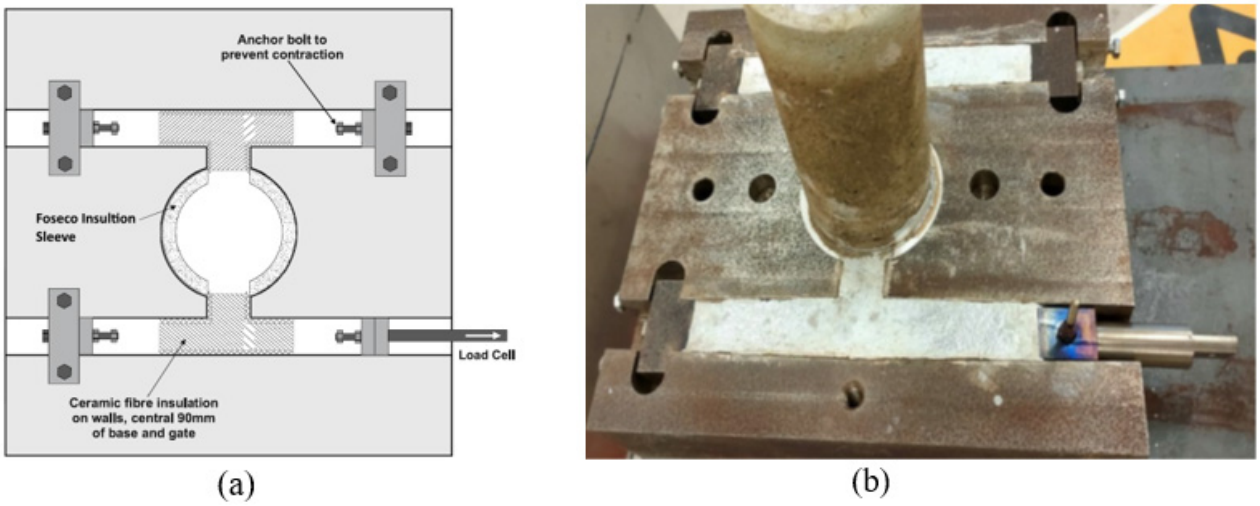

Figure 1: (a) Plan view of the mould [16, 19, 20] and (b) casting with mould.

FEA Model

In this study, the ProCAST virtual casting software tool [28] has been used to simulate the stress and strain development, and the hot tearing formation. Figure 2 shows the CAD model of the CHT (cast hot tearing) rig. The base is divided into three opposite parts, forming an H-shaped empty bin after splicing, which can cope with different heat transfer conditions between different parts of the casting and the mould. The same material data and boundary conditions were used for each case simulated, except of course for the alloying percentage. The FEA model itself is largely created automatically by ProCAST's VISUAL meshing and modelling tool

whose user interface has a casting industry focus. One imports a CAD model of the part, cleans up any small irregularities in the CAD model, and then defines the components of the casting within that CAD model, discretizing this into 761,821 tetrahedral elements and 139,755 nodes. The quality of the meshes was checked to achieve the required convergence.

Heat transfer coefficient: In Figure 2a, two distinct sets of interfacial heat transfer coefficients have been designated for the mould-to-casting interface to replicate the intended experimental rig configuration. The far ends of the bars, depicted in white, have been assigned an interfacial HTC1 of 500 W/m²·K, while the central portion, highlighted in red, has an HTC2 of 200 W/m²·K.

Restrained surfaces for stress simulation: As depicted in Figure 2b, mirroring the authentic casting procedure, solely one end is affixed to a dynamometer to gauge load, whereas the remaining three ends are constrained from displacement.

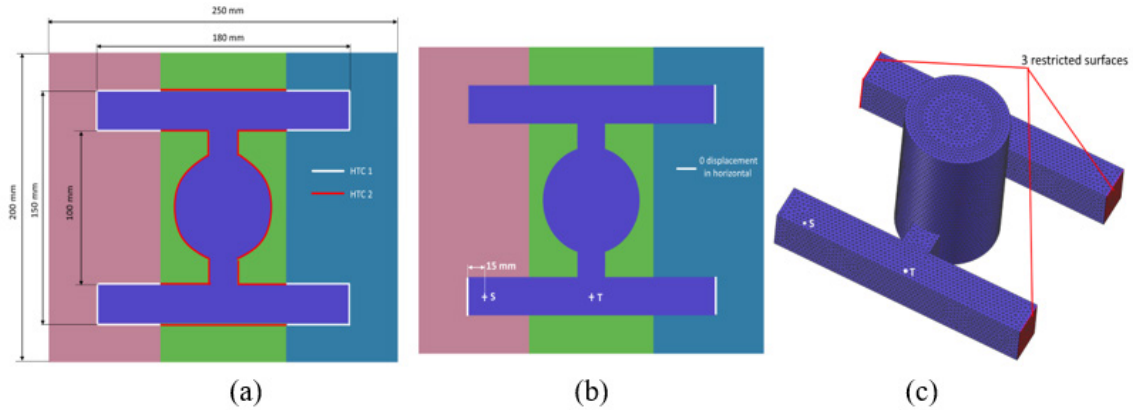

Figure 2: The heat transfer coefficient setting separately of the four end regions and the cen-tral region, (a) two interfacial heat transfer coefficients, (b) and (c) restricted surfaces (T re-fers to the node at which the hot spot temperature was measured, and S to refers the node at which the end stress of the bar was measured).

Material model: In this study, an Elasto-Plastic model was employed to simulate stress and strain. Specifically, the Elastic model incorporated thermal expansion coefficients, Young's modulus, and Poisson's ratio and the Plastic model incorporated yield stress and the hardening coefficient. The material properties defined for both the Elastic and Plastic models varied with temperature. The linear hardening is defined as follows [28]:

$$\sigma = \sigma_0 + H\varepsilon^{pl}, \qquad (1)$$

here, σ_0 is yield stress, ε^{pl} is plastic strain, and H is the plastic modulus.

To determine the material properties for the three alloys, ThermoCalc was utilized, with the thermal properties data calculated using the back diffusion model [29]. Additionally, the solid fraction profile for each alloy was obtained from MatPro® utilizing the Thermotech TT-Al database under back diffusion conditions.

Hot tearing criteria: The hot tearing indicator (HTI) has been used to predict hot tearing. This model is based upon the total strain which occurs during solidification [28], i.e. it is "strain driven" in that it computes the elastic and plastic strain at a given location (or node) when the fraction of solid is between CRITFS (usually 50%) and 99%. The HTI is computed based on the Gurson Damage Model [28]. It is defined by accumulated plastic strain in the mushy zone that corresponds to the void nucleation described in that model:

$$HTI = \bar{\varepsilon}^{p}_{ht} = \int_{t_c}^{t} \dot{\varepsilon}^{p}\, dt \qquad t_c \le t \le t_s \qquad (2)$$

Here, $\bar{\varepsilon}^{p}_{ht}$ is the critical accumulated effective plastic strain for the initiation of hot tearing, $\dot{\varepsilon}^{p}$ is the effective plastic strain rate, t_c denotes the time when the coherency temperature is reached, and t_s is the time when the solidus temperature is reached.

Results

Load and Stress Development

Figure 3 shows the load measurements obtained from the experimental setup and the temperature data recorded by the hot spot thermocouple, alongside the simulated temperature profiles and solid fraction distributions at the specific location of the test bar. Additionally, the effective stress values at the end of the cast bar are presented. Looking at the low solute alloy, Al-0.5wt% Cu, depicted in Figure 3a, the progression of load initiation is observed during the primary α-phase of aluminium solidification, culminating in a rapid escalation to 775N within a concise timeframe of 68 seconds post-solidification. In contrast, for the higher solute alloys, Al-3wt% Cu and Al-5wt% Cu depicted in Figures 3b and Figures 3c, the load development is instigated subsequent to a phase of rapid cooling, eventually reaching levels of 800N and 875N at 70 seconds and 75 seconds, respectively. Looking again at the Al-0.5wt% Cu alloy, its solidification behaviour shows a remarkable decline in solid fraction from 0.1 to 1 at a critical temperature of 650°C, accomplished in a mere 2 seconds. Again in contrast, the solidification kinetics for Al-3wt% Cu and Al-5wt% Cu alloys necessitate 48 seconds and 75 seconds, respectively, to attain complete solidification from a solid fraction of 0.1 to 1.

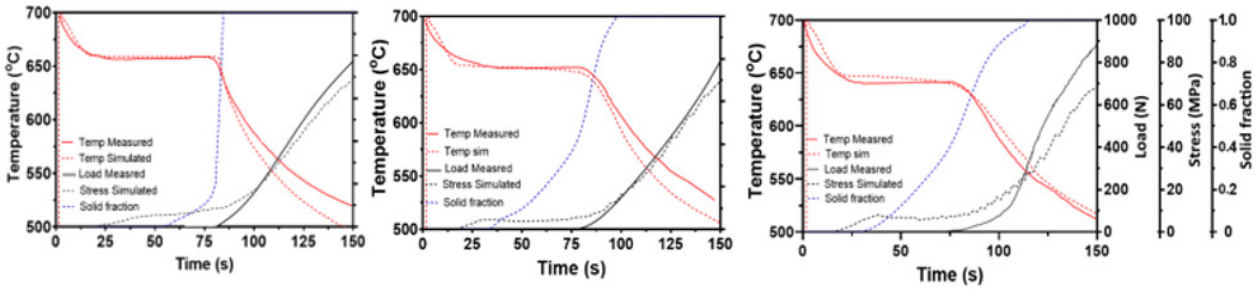

Figure 3: Simulated hot spot temperature and the stress at the end of the bar.

(a) Al-0.5Cu alloy (b) Al-3Cu alloy (c) Al-5Cu alloy

Comparing actual data with simulated data, it is evident that temperature fluctuations closely align with the measured values. However, the simulated stress exhibits a distinct behaviour, gradually escalating during the isothermal solidification phase, reaching 10MPa before experiencing a rapid surge to 70MPa post-isothermal solidification completion. In contrast, the actual load manifests post-isothermal process, exhibiting a rapid rise inversely correlated with the temperature decline. Although direct comparison between simulated stress and actual load proves challenging due to their disparate nature as distinct quantities, they nonetheless exhibit analogous developmental trends. The gradual increase in the actual measured load might have encountered some delay owing to frictional forces between the test components and the mould, yet this didn't significantly alter the overarching trend.

Both experimental findings and simulation outcomes reveal a discernible deceleration in the solidification rate of aluminium alloy as the copper content escalates. The Al-0.5wt% Cu alloy achieves full solidification within 20 seconds, contrasting with the Al-3wt% Cu and Al-5wt% Cu alloys, which require extended times of 50 seconds and 80 seconds, respectively. Moreover, the Cu content has the same effect on the load, and as the Cu content increases. Specifically, load values elevate to 775N, 800N, and 875N at time intervals of 150 seconds for alloys with increasing copper content, respectively.

Hot tearing and HTI

Figure 4 shows the observed hot tearing phenomenon in the cast rod and the distribution of HTI in the simulation of the studied Al-Cu alloy. According to Figures 4a_1 and Figures 4b_1, significant thermal tearing occurred in Al-0.5wt% Cu and Al-3wt% Cu, with cracks penetrating the entire cast bar. In the case of the low-solute alloy comprising 0.5wt% Cu, the crack width measures approximately 1.8mm and is accompanied by numerous smaller cracks at its termination. Interestingly, in the case of the high-solute alloy comprising 3wt% Cu, the crack width is narrower, measuring only 0.5mm, although it too is accompanied by multiple smaller cracks. Conversely, as seen in Figure 4c_1, the high-solute alloy with 5wt% Cu shows no significant thermal tearing phenomenon.

Figures 4a_2 –c_2 show the HTI distribution of the aluminium alloy at the end of the solidification process during the simulation. The content of Cu in the alloy has a direct impact on that HTI distribution. The low solute alloy 0.5wt% Cu has the peak of HTI appearing in the centre of the casting bar, at approximately 0.022, it being quite concentrated. The high solute alloy 3wt% Cu and 5wt% Cu have their peak HTI appear in the centre of the cast bar and the two corners of the joints, at approximately 0.022 and 0.03 respectively, and although in contraction, the peaks vary slightly.

This means that as the Cu content in the aluminium alloy increases, the peak distribution of HTI becomes more dispersed, gradually shifting from the central position to the corner positions of the connection. Nevertheless, the peak at the central position can still be maintained at about 0.02, and the area of each peak range increases with the Cu content, and the peaks around it have a much closer value and a larger area.

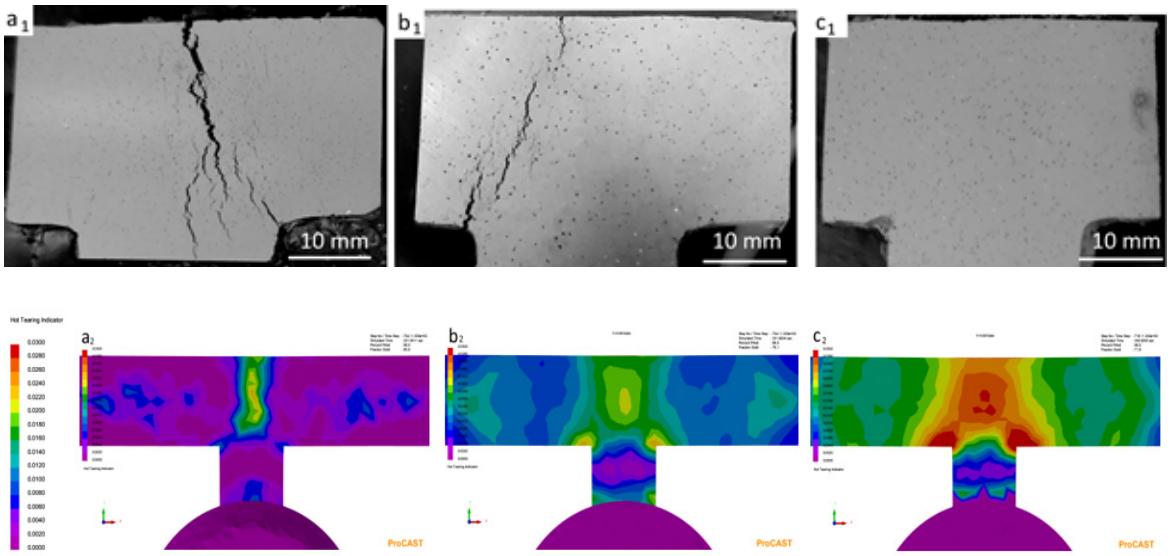

Figure 4: Photographs of hot tearing in (a1) Al-0.5wt%Cu, (b1) Al-3wt%Cu and (c1) Al-5wt%Cu alloy; and simulated HTI in (a2) Al-0.5wt%Cu, (b2) Al-3wt%Cu, and (c2) Al-5wt%Cu.

Development of Stress, Strain, and Formation of Hot Tearing

Figure 5 shows the longitudinal simulation data over time for three aluminium alloys with different copper contents, including temperature, solid fraction, effective stress, effective strain, and HTI curves. In Figures 5a_1-c_1, it is quite clear that there is a significant difference between the temperatures at the distal and central regions, and that this difference decreases with the increase of Cu content. At 84.5 seconds, the temperature difference between the distal and central temperatures of Al-0.5wt% Cu is about 175°C, while Al-3wt% Cu and Al-5wt% Cu are 135°C and 100°C, respectively. In Figures 5a_2-c_2, the solidification of all alloys gradually diffuses from the far end to the centre. Al-0.5wt% Cu achieved complete solidification after 84.5 seconds, which is much faster than the 98 seconds of Al-3wt% Cu and the 118 seconds of Al-5wt% Cu. The stress corresponding to the solidification also accumulates from the far end and extends to the centre, and the stress peaks of all alloys appear near the far end of the casting rod. The effective stress peaks of Al-0.5wt% Cu appear at 15-25mm and 150-160mm, and continue to increase with the increase of solidification. The effective stress peaks in Al-3wt% Cu are at 15-30mm and 150-170mm, and Al-5wt% Cu at 15-40mm and 140-170mm. These two high solute alloys accumulate additional effective stress peaks towards the centre position as solidification progresses, resulting in a wider distribution of effective stresses. However, it is worth noting that the highest effective stress peak value in Al-5wt% Cu alloy ultimately appeared at around 50mm and 120mm near the centre, at approximately 27.5MPa, which is the highest effective stress peak among the three alloys.

As the solidification increases, the effective strain of the three alloys gradually accumulates (symmetrically). The first peak of Al-0.5wt% Cu is 0.01 at 48.5 seconds, and as the solidification progresses towards the centre, the effective strain gradually increases and different peaks

appear. The strain at the centre position (80mm-100mm) rapidly increases from 0 at 80.5 seconds to 0.0225 within 4 seconds. During the initial solidification stage, Al-3wt% Cu exhibits a peak of 0.01 at 50mm (58 seconds) and a slight decrease at 50mm-70mm. At the centre position (70mm-110mm), the solid fraction exceeds 50%, and there is an effect change from 0 to 0.0225, which is the same as the effective strain of Al-0.5wt% Cu, but it takes 20 seconds. Al-5wt% Cu reaches a peak of 0.015 at 45mm and ultimately reaches 0.0275 (116.8 seconds) at the centre. By comparison, with the increase of copper content, the increase in effective strain at the centre position gradually becomes gentle, but Al-5wt% Cu has the highest peak.

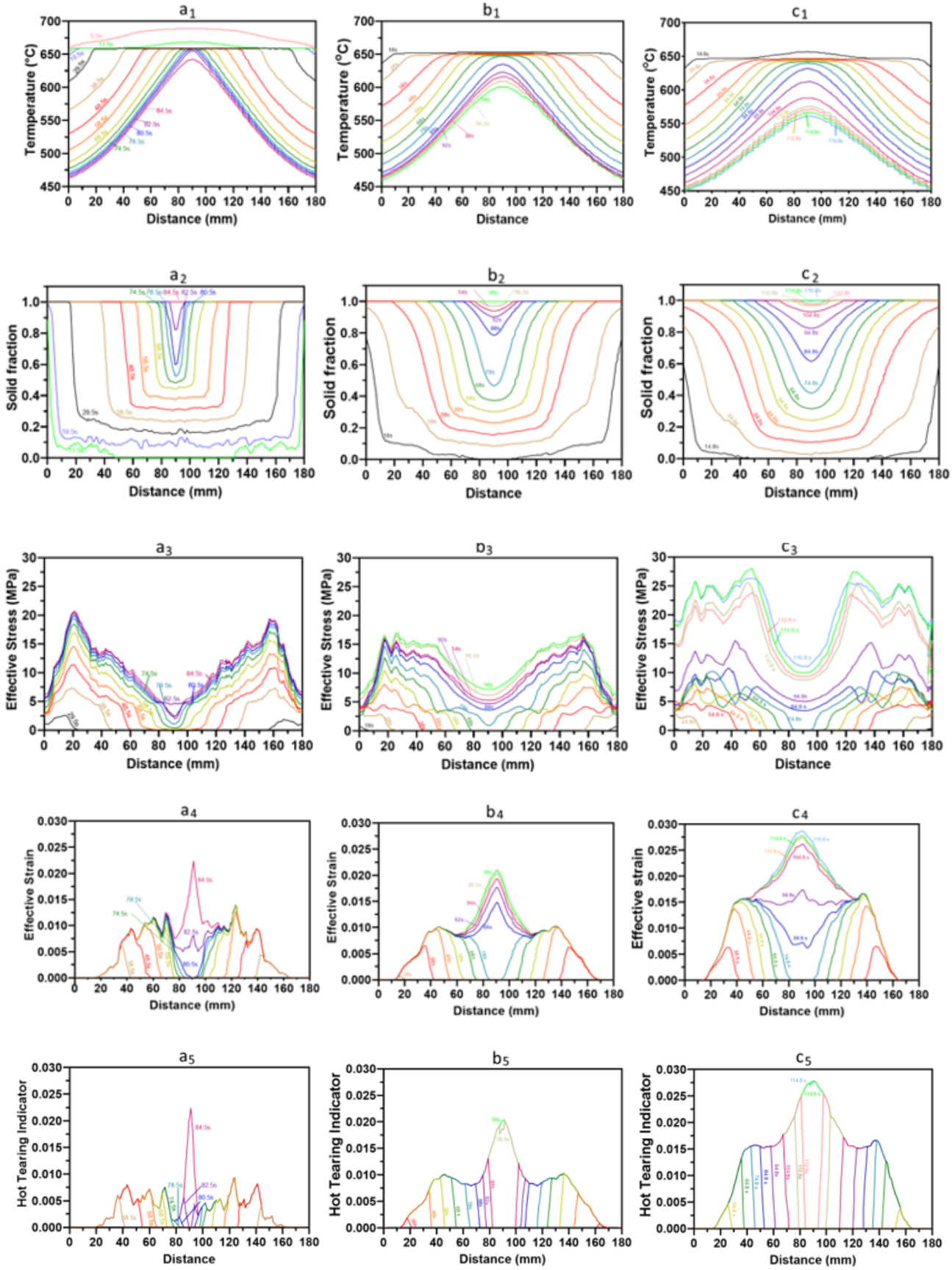

Figure 5: Simulated evolution of temperature, solid fraction, effective stress, effective strain and HTI of (a) Al-0.5wt%Cu, (b) Al-3wt%Cu, and (c) Al-5wt%Cu alloys.

The progress of HTI at different positions follows a pattern similar to the effective strain, but the three alloys show significant differences but also exhibit left-right symmetry. Al-0.5wt% Cu exhibits multiple peaks at both ends and reaches 0.0225 in the final solidification stage (solid fraction exceeding 60%), indicating a narrow distribution of its HTI peak. Al-3wt% Cu gradually increases to a weak peak, then slightly decreases, and finally rises to 0.020, but the rate of increase is significantly lower than Al-0.5wt% Cu. The changes in Al-5wt% Cu and Al-3wt% Cu are similar, but the overall values are relatively high, reaching a weak peak of 0.0155. After a slight decrease, they finally rise to 0.0275. By comparing the cracks generated by actual casting rods, it was found that the relatively uniform distribution of HTI in the direction of elongation and solidification may more likely be the key to reducing the thermal tearing of Al Cu alloy than the value of HTI.

Discussion

As shown in Figure 5, the simulations revealed that there are significant differences between the three alloys in temperature gradient, solid fraction, effective stress and strain, and HTI in the last few seconds before the solidification in the hot spot when the hot tearing occurs. These differences may be useful to explain the mechanism of the hot tear formation for these binary alloys.

Temperature Gradient, Cooling Rate, and Solid Fraction at The Hot Spot Region

Figure 6a shows temperature gradient and cooling rate extracted from the simulated temperature at the hot spot at the time it was solidified. Both temperature gradient and cooling rate at the hot spot decreased with the Cu increase, the temperature gradient decreasing from 2.0, to 1.6, and finally to 1.0°C/mm while the cooling rate decreasing from 1.25, to 0.8 and finally to 0.5°C/s.

Strain, Strain Rate, Strain Gradient, and HTI

In Figures 6b and 6c, effective strain, strain rate, strain gradient (the rate of change of the effective strain with distance), and the HTI at the hot spot in the last moment of the solidification are plotted against Cu content for the three alloys. In effective plastic strain was 0.028, higher than that of Al-0.5wt%Cu (0.022) and Al-3wt%Cu (0.020) which were much the same. The well-designed feeding hot spot in this study has a strain rate of 0.0055/s for Al-0.5%Cu alloy, much higher than the 0.00035/s of Al-3wt%Cu and the 0.0005/s of Al-5%Cu. The strain gradient decreased with the increase of Cu content, from 0.0014 of Al-0.5wt%Cu, 0.00065 of Al-3wt%Cu, to 0.00014 for Al-5wt% Cu as shown in Figure 6b.

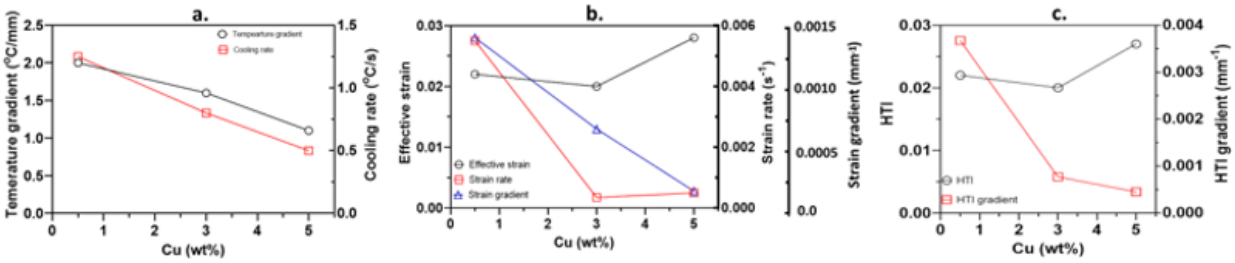

Figure 6: (a) Temperature gradient and cooling rate, (b) effective strain and strain rate, and (c) HTI and HTI gradient against Cu content.

As Figure 4 shows, the HTI is the highest at the hot spot where the hot tearing occurred. However, as recommended in ProCAST Manual [28] the HTI value cannot be compared between different alloys. In this study, the Al-0.5wt%Cu and Al-3.0wt%Cu alloys with lower HTIs of 0.022 and 0.020 exhibited hot tearing while the HTI 0.28 of the Al-5wt%Cu alloy did not. The differences of the HTI gradient against the longitude between the experimental alloys show that the HTI gradient for Al-3wt%Cu reaches 0.0007 which is significantly lower than 0.0037 for the Al-0.5wt%Cu alloy but not much different from 0.0005 for Al-5wt%Cu.

Hot tearing theories have been proposed based on the understanding of the stress and strain development during the solidification. Early theories were based on strain accumulation in hot spot regions, but subsequent studies have suggested that strain rate rather than actual strain was the critical parameter for hot tearing. Sistaninia et al. [30] have further demonstrated that the dependence of hot tearing on either strain or strain rate is associated with the feeding condition of the mushy zone. When the mushy zone can be fed sufficiently, the critical factor for hot tearing is strain rate, but conversely, when the mushy zone cannot be fed sufficiently, hot tearing will also be affected by strain accumulation.

The large differences in both strain rate and strain gradient in the Al-0.5wt%Cu and Al-5wt%Cu alloys agree with the occurrence of hot tearing. However, very little difference is found between the Al-3wt%Cu and Al-5wt%Cu alloys on either strain rate or strain gradient, an indication that the complexity of the hot tearing and alloy-dependent phenomenon being one with many variables influencing its formation.

Correlation of Stress and Strain Development at The Hot Spot and the End of the Test Bar

Figure 7 shows the evolution of temperature, solid fraction, stress and strain at both the hot spot and the end of the test bar. The temperature at the end of the bar drops rapidly as shown in Figures $7a_1$ and $7a_2$ for the Al-0.5wt%Cu alloy, where the solidification started at 16 seconds and was completed at 20 seconds. The stress started to build up once solidification was completed at 20 seconds and gradually increased to 5MPa within 20 seconds, with no significant increase until 90 seconds. No strain was developed at the end of the bar. On the other hand, the temperature at the hot spot changed more slowly, the solidification started at 54 seconds and was completed at 83 seconds. The stress started to build up at 80 seconds when the solid fraction was about 0.20, with full solidification taking a further 4 seconds, by which time the stress had increased to 3MPa. Strain also starts at 80 seconds and rises linearly to 0.09 in 4 seconds.

Increasing Cu content to 3.0wt% and 5.0wt% saw solidification at the end of the test bar begin at 12 seconds and 10 seconds and be completed at 32 seconds and 45 seconds. The stress of the Al-3wt%Cu and Al-5wt%Cu alloy started at 19 seconds and 18 seconds when the solid fraction had reached 0.5 and 0.4 respectively. It then increased to 3MPa and 10 MPa at 40 seconds and remained so for 40 seconds. Similarly, no strain occurred.

The solidification at the hot spot started at 35 seconds and 30 seconds and ended at 98 seconds and 114 seconds for Al-3wt%Cu and Al-5wt%Cu alloys as seen in Figure 7b and Figure 7c. The stress of Al-3wt%Cu started at 80 seconds when the solid fraction

was 0.5 and reached 5MPa when fully solidified, while the strain appeared at 82 seconds when the solid fraction was 0.6 and increased rapidly to 0.017 within 16 seconds of full solidification. The strain of Al-5wt%Cu also appeared at 80 seconds and the solid fraction was the same at 0.5 and increased slowly within 34 seconds of full solidification to 10 MPa. The strain of Al-5wt%Cu also occurs at 80 seconds when the solid fraction is 0.5, which increases slowly to 10 MPa within 34 seconds of complete solidification, and the strain also occurs at 82 seconds, but the solid fraction is slightly lower than 0.6 and finally reaches 0.022 at the completion of solidification.

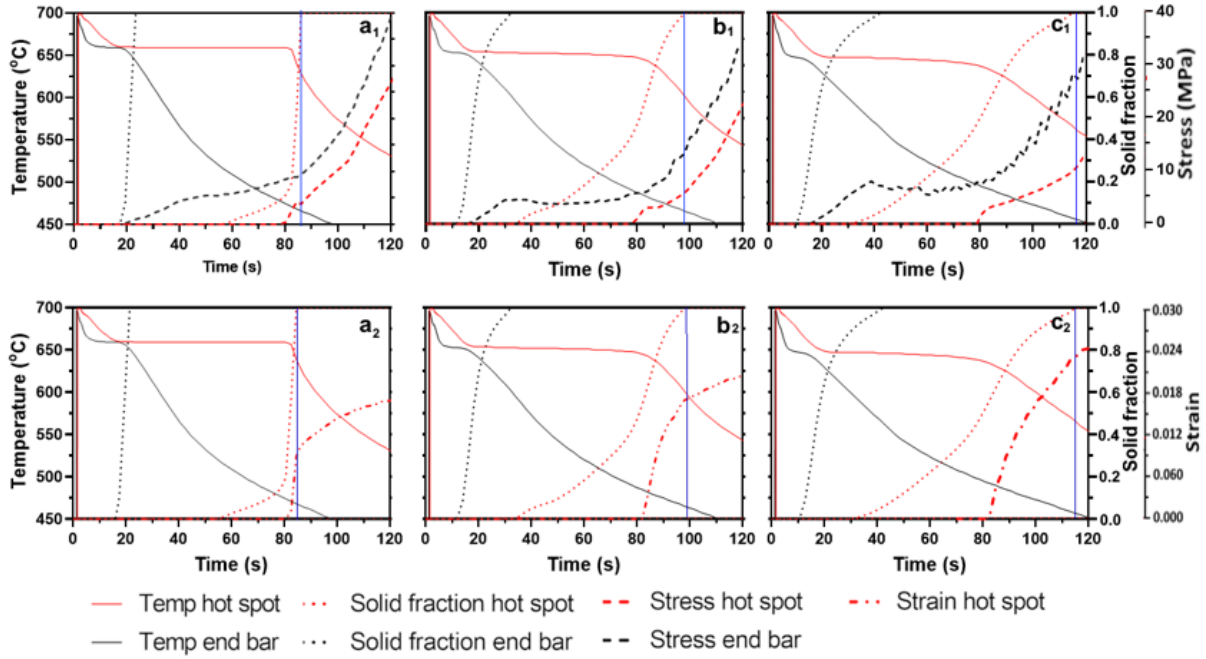

Figure 7: Stress and strain development at the hot spot (in black) and the end bar (in red). (a) Al-0.5wt%Cu; (b) Al-3.0wt%Cu; and (c) Al-5.0wt%Cu.

Past work demonstrated that the observed increase in the load at the Non-Equilibrium Solidus (NES load) can serve as an indicator of their hot tearing susceptibilities, and that this NES load mirrored the amount of the unfed shrinkage and thus was related to the pressure drop in the mushy zone [12,25,31]. For the current setup, there is no correlation on the stresses and strain development between the hot spot and the end of the test bar. Due to the qualitative comparison between load measured and stress simulated, it is concluded that there is no relationship between load value and hot tearing susceptibility.

Even through no quantitative comparisons between the measured load and the simulated stress can be made because they are different quantities, the trend is the same, indicating that they are qualitatively comparable. The starting stress is earlier than that of measured load, which may have been due to the friction between the slide and mould surface in the experiments. The load measured and stress simulated may not be directly related to the stress and strain development in the hot spot of the centre of the test bar. The relationship between the end and the centre of the bar needs to be further investigated and clarified.

Conclusions

Numerical experiments (i.e. simulation) and physical experiments were used to investigate the hot tearing susceptibility of Al-Cu binary alloys with solute contents of 0.5, 3.0, and 5.0wt% Cu. The following conclusions about the influence of Cu composition can be made in respect of the hot tearing susceptibilities during the casting of these alloys: Large tears in the Al-0.5wt%Cu alloy are present. In the Al-3wt%Cu alloy, the primary tear is significantly smaller, and in the Al-5wt%Cu alloy, there was no sign of hot tearing. The Al-0.5wt%Cu and Al-3.0%Cu alloys with lower HTIs of 0.022 and 0.020 exhibited hot tearing while the Al-5wt%Cu alloy with a HTI of 0.28 did not. The differences of the HTI gradient against the longitude between the three experimental alloys show that the HTI gradient reaches just 0.0007 for Al-3wt%Cu, significantly lower than the 0.0037 for Al-0.5wt%Cu but not much different from the 0.0005 for Al-5wt%Cu.

Simulations show that in the last moments before solidification was complete, both the temperature gradient and cooling rate at the hot spot dropped with the Cu increase, in particular, the temperature gradient dropped from 2.0, 1.6, to 1.0°C/mm while the cooling rate dropped from 1.25, 0.8 to 0.5°C/s. The broader region of slower solidification growth of the Al-5wt%Cu alloy leads to a higher permeability in the mushy zone, so therefore a higher ability to heal micro-pores and reduce hot tearing susceptibility. In comparison, the quicker increase in solid fraction over a narrower band for the lower solute content alloys translates into an order of magnitude drop in permeability in the last stages of solidification, leading to a lower ability to heal micro-pores. There is not much difference in effective strains between the three alloys. Interestingly though, the Al-0.5wt%Cu alloy showed both a much higher strain rate at the hot spot of the test bar than that of the Al-3wt%Cu and Al-5wt%Cu alloys, as well a higher strain gradient along the longitudinal direction.

It is believed that the low permeability, high strain rate, and high strain gradient in the last moment of solidification are attributable to the formation of hot tears in the Al-0.5wt%Cu alloy. However, very little difference is found between Al-3wt%Cu and Al-5wt%Cu on either strain rate or strain gradient indicating the complexity of the hot tearing and alloy-dependent phenomenon with many variables influencing its formation. Simulations also indicated that there is no correlation on the stresses and strain development between the hot spot and the end of the test bar for the CHT rig used in this study. Due to the qualitative comparison between load measured and stress simulated, it is also concluded that there is no relationship between load value and hot tearing susceptibility.

Acknowledgments

This research was funded by the Baosteel-Australia Joint Centre (BAJC), grant number BA19017. Technical support from the team at Pacific Engineering Systems International is also acknowledged.

References

1. Climate Action Pathway Transport Executive Summary.
2. Kupfer R, Schilling L, Spitzer S, Zichner M, Gude M (2022) Neutral lightweight engineering: a holistic approach towards sustainability driven engineering. Discover Sustainability 3(1): 17.
3. Czerwinski F (2021) Current trends in automotive lightweighting strategies and materials. Materials 14(21): 6631.
4. Fiedler F, Bergweiler G, Burggräf P, G Schuh (2022) Fields of Action in Mega-Casting for the Industrializiation of Automotive Car Bodies. ed: Unpublished.
5. Baser TA, Elif U, Akinci V (2022) New trends in aluminum die casting alloys for automotive applications. The Eurasia Proceedings of Science Technology Engineering and Mathematics 21: 79-87.
6. Yang B, Wu J, Zeng Y, Liu J, Yang N, et al. (2024) Hot Tear Formation During the Casting of Al–Zn Binary Alloys. Advanced Engineering Materials 26(2): 2301471.
7. Sun X, Han X, Dong C, Li X (2021) Applications of aluminum alloys in rail transportation. Advanced Aluminum Composites and Alloys 9: 251-268.
8. Eskin D, Katgerman L, Suyitno, Mooney JF (2004) Contraction of aluminum alloys during and after solidification. Metallurgical and Materials Transactions A 35: 1325-1335.
9. Eskin DG, Katgerman L (2006) Thermal contraction during solidification of aluminium alloys. Materials science forum 519-1521: 1681-1686.
10. Eskin D, Katgerman L (2004) Mechanical properties in the semi-solid state and hot tearing of aluminium alloys. Progress in materials science 49(5): 629-711.
11. Jarry P, Rappaz M (2018) Recent advances in the metallurgy of aluminium alloys. Part I: Solidification and casting. Comptes Rendus Physique 19(8): 672-687.
12. Li Y, Li H, Katgerman L, Du Q, Zhang J, et al. (2021) Recent advances in hot tearing during casting of aluminium alloys. Progress in Materials Science 117: 100741.
13. Dantzig JA Rappaz M (2016) Solidification: -Revised & Expanded. EPFL press.
14. Stangeland A, Mo A, M'Hamdi M, Viano D, Davidson C (2006) Thermal strain in the mushy zone related to hot tearing. Metallurgical and Materials Transactions A 37: 705-714.
15. Han Q, Hassan M, Viswanathan S, Saito K, Das S (2004) An experimental method for determining mechanical properties in the non-equilibrium mushy zones of alloys. In MG Chu, DA Granger, Q Han (Eds.) Solidification of Aluminum Alloys. 211-220.
16. Instone S, StJohn D, Grandfield J (2000) New apparatus for characterising tensile strength development and hot cracking in the mushy zone. International Journal of Cast Metals Research 12(6): 441-456.
17. Kumar A, Založnik M, Combeau H, Lesoult G, Kumar A (2021) Channel segregation during columnar solidification: Relation between mushy zone instability and mush permeability. International Journal of Heat and Mass Transfer 164: 120602.
18. Viano D, StJohn D, Grandfield J, Cáceres C (2016) Hot Tearing in Aluminium-Copper Alloys. Essential Readings in Light Metals: Volume 3 Cast Shop for Aluminum Production 895-899.
19. Viano D (2021) Hot tearing in aluminium alloys, PhD thesis. The University of Queensland Australia.
20. D'Elia F, Ravindran C, Sediako D, Kainer K, Hort N (2014) Hot tearing mechanisms of B206 aluminum-copper alloy. Materials & Design 64: 44-55.
21. Sistaninia M, Terzi S, Phillion A, Drezet J M, Rappaz M (2013) 3-D granular modeling and in situ X-ray tomographic imaging: A comparative study of hot tearing formation and semi-solid deformation in Al-Cu alloys. Acta materialia 61(10): 3831-3841.
22. Ludwig O, Drezet JM, Martin CL, Suéry M (2005) Rheological behavior of Al-Cu al-loys during solidification constitutive modeling, experimental identification, and numerical study. Metallurgical and Materials Transactions A 36: 1525-1535.
23. Suyitno, Savran V, Katgerman L, Eskin D (2004) Effects of alloy composition and casting speed on structure formation and hot tearing during direct-chill casting of Al-Cu alloys. Metallurgical and Materials Transactions A 35: 3551-3561.
24. Ju Y, Arnberg L (2003) Measurement of grain bridging in some Al-Cu and Al-Sn alloys. International Journal of Cast Metals Research 16(6): 522-530.
25. Li Y, Zhang ZR, Zhao ZY, Li HX, Katgerman L, et al. (2019) Ef-fect of main elements (Zn, Mg, and Cu) on hot tearing susceptibility during direct-chill casting of 7xxx aluminum alloys. Metallurgical and Materials Transactions A 50: 3603-3616.
26. Li S, Sadayappan K, Apelian D (2013) Role of grain refinement in the hot tearing of cast Al-Cu alloy. Metallurgical and Materials Transactions B 44: 614-623.
27. Y Li, Bai QL, Liu JC, Li HX, Du Q, et al. (2016) The influences of grain size and morphology on the hot tearing susceptibility, contraction, and load behaviors of AA7050 alloy inoculated with Al-5Ti-1B master alloy. Metallurgical and Materials Transactions A 47: 4024-4037.
28. ESI Group Inc. ProCAST 2020.0 User Guide ESI Group Inc 2020.
29. Guo J, Samonds M (2007) Alloy thermal physical property prediction coupled computational thermodynamics with back diffusion consideration. Journal of phase equilibria and diffusion 28: 58-63.
30. Sistaninia M, Phillion A, Drezet JM, Rappaz M (2012) A 3-D coupled hydromechanical granular model for simulating the constitutive behavior of metallic alloys during solidification. Acta materialia 60(19): 6793-6803.
31. Y Li, Gao X, Zhang ZR, Xiao WL, Li HX, et al. (2017) Experimental and Theoretical Studies of the Hot Tearing Behavior of Al-x Zn-2Mg-2Cu Alloys. Metallurgical and Materials Transactions A 48: 4744-4754.